Vol 16 No 6, June 2007
1009-1963/2007/16(06)/1731-05
Chinese Physics
© 2007 Chin. Phys. Soc.
and IOP Publishing Ltd

Micromagnetic simulation for high field sensors with perpendicular magnetizations*

Jin Wei(金 伟)[a)b)] and Liu Yao-Wen(刘要稳)[a)†]

[a)] *Department of Physics, Tongji University, Shanghai* 200092, *China*

[b)] *College of Physics and Communication Electronics, Anhui Normal University, Wuhu* 241000, *China*

(Received 23 September 2006; revised manuscript received 28 November 2006)

In this paper, we present a micromagnetic design for high field sensors. The hard layer of the sensors is $L1_0$–FePt which is magnetized perpendicularly to film plane and the sense layer is NiFe which is magnetized in the film plane. The magnetization configurations of the hard and sense layers at different external magnetic fields have been simulated. In micromagnetic simulation, the sense field up to one tesla can be reached by using this sensor. We find that whether the sensor has a symmetric or an asymmetric field-sensing window is determined by the coercive field of the hard layer and the demagnetizing field of the sense layer.

Keywords: micromagnetic simulation, giant magnetoresistive, coercivity, demagnetizing field
PACC: 7000, 7500, 7570P, 7540M

1. Introduction

Giant magnetoresistive (GMR) sensors such as magnetic spin-valves and magnetic tunnel junctions (MTJs) are widely used as sensing elements in low magnetic field measurements in the range of 0.01–100 Oe ($0.8 - 8000$ A/m, 1Oe = 80 A/m).[1−4] One of the most commercialized applications of GMR sensors is the reading head of hard-disk drive. However, in some other applications such as magnetic levitating train and positioning sensor, the sensing field is typically from several to tens of kOe. Thus high-field sensors are required. Currently, Hall sensors are used in these areas. But they have shortcomings such as poor thermal stability (< 150 °C) and limited operation frequency range (< 10 kHz), which restricts their wide applications. Recently, high-field GMR sensors were proposed as promising candidates to solve the problems.[5,6] A high-field GMR sensor is typically designed in the following way. It uses a ferromagnet with perpendicular anisotropy as the hard layer and another ferromagnet with in-plane anisotropy as the sense layer. In this article, a micromagnetic simulation of such sensors is presented.

2. Simulation model

As shown in Fig.1, $\boldsymbol{M}_1$ is the hard layer, which has a large perpendicular magnetic anisotropy creating an easy axis along the film normal (z axis direction). $\boldsymbol{M}_2$ is the sense layer, which has an in-plane anisotropy. The materials of $\boldsymbol{M}_1$ can be chosen from TbFe alloys, FePt alloys or Pt/Co multilayers.[5−9] In this simulation $\boldsymbol{M}_1$ is assumed to be $L1_0$–FePt and $\boldsymbol{M}_2$ is NiFe. The magnetic field is applied to the film normal (z axis).

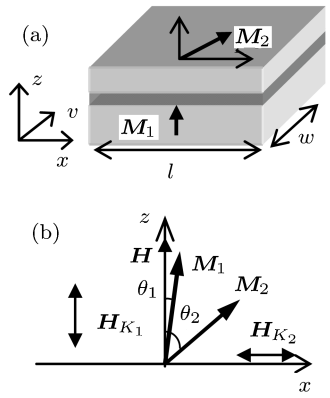


Fig.1. Schematic drawing of a high magnetic field spin-valve sensor: (a) structure, and (b) magnetization and anisotropy directions. The magnetic field is applied to the film normal.

The magnetization response of the spin valve sensor to the field can be obtained by minimizing the total energy, which can be written as a sum of anisotropy, Zeeman, demagnetization, intralayer exchange and interlayer exchange energies. Each magnetic layer (hard

*Project supported by the Nature Science Foundation of China (Grant No 10404019) and by the Science and Technology Committee of Shanghai (Grant No 05PJ14090).
†Corresponding author. E-mail: yaowen@mail.tongji.edu.cn

and sense) is discretized into a two dimensional array of mesh cells. Each cell is 5 nm × 5 nm. The detailed micromagnetic method can be found in our previous works.[10−12]

When a magnetic field $\boldsymbol{H}_{\rm a}$ is applied along the z axis, the in-plane magnetized layer $\boldsymbol{M}_2$ rotates towards the external field direction while the perpendicularly magnetized layer $\boldsymbol{M}_1$ remains in the fixed direction, resulting in the resistance change of the sensor (i.e. GMR output) as a function of the external field:[5]

$$R(H) = R_{\rm P} + (1/2)(R_{\rm AP} - R_{\rm P})(1 - \langle\cos(\theta_1 - \theta_2)\rangle), \quad (1)$$

where θ_1 and θ_2 are the angles of $\boldsymbol{M}_1$ and $\boldsymbol{M}_2$ for each discrete cell with respective to the direction of external field, as shown in Fig.1(b), and the $\langle\cdots\rangle$ denotes the average which is taken over all the mesh cells. $R_{\rm ap}$ and $R_{\rm p}$ are the resistance of sensor for the $\boldsymbol{M}_1$ and $\boldsymbol{M}_2$ in antiparallel and parallel alignments, respectively.

3. Results and discussion

The simulated transfer curves as a functions of the magnetic field are shown in Fig.2(a). Figures 2(b)–2(i) show the magnetization configurations of the two layers during the switching loop. The simulation was carried out for a sensor element with the structure of FePt 30Å/Cu 25Å/NiFe 30Å, with the lateral dimension of 1×1 μm^2. The material parameters are chosen as $K_1 = 1.2 \times 10^7$ erg/cm^3 (1.2 J/cm^3) and $M_{\rm s} = 1100$ emu/cm^3 (1.1×10^6 A/m) for $\boldsymbol{M}_1$ layer, which are typical values of $L1_0$-ordered FePt alloy.[9] For $\boldsymbol{M}_2$ layer (i.e. NiFe), we use the typical values of $K_2 = 5 \times 10^3$ erg/cm^3 and $M_{\rm s} = 800$ emu/cm^3. In this simulation, the positive magnetic field is defined along $+z$ direction. The sweeping direction of the magnetic field is indicated by alphabets A through I. At a high field $H = 15$ kOe in the $+z$ direction, both layers are saturated in the field direction, as shown in Fig.2(b). In such a parallel configuration, the sensor has a low resistance. This configuration remains almost the same until the field is decreased to ~ 10 kOe (step $A \rightarrow B$). After that, the magnetization of $\boldsymbol{M}_2$ starts to rotate towards the in-plane direction due to the in-plane crystalline anisotropy and the demagnetization field. However, the magnetization of $\boldsymbol{M}_1$ still keeps $+z$ direction due to its large perpendicular anisotropy ($2K_1/M_1 \approx 21$ kOe). As a result, a linear increase of the sensor resistance is observed (steps $B \rightarrow C$). Figure 2(c) shows the complete in-plane magnetization configuration of M_2 occurring at zero field. When the magnetic field is switched to the negative direction ($C \rightarrow D$), $\boldsymbol{M}_2$ rotates towards the $-z$ direction while $\boldsymbol{M}_1$ still remains in $+z$ direction. As a result, the resistance further increases and reaches the maximum value at $H = -8.2$ kOe, where the magnetizations of $\boldsymbol{M}_1$ and $\boldsymbol{M}_2$ are almost antiparallel (AP), see Fig.2(d). At $H = 8$ kOe, a sharp switching from high-resistance state to low-resistance state is observed, because the magnetization of $\boldsymbol{M}_1$ reverses its direction [Fig.2(e)]. We infer that the external field surpasses the coercive field $H_{\rm c1}$ of $\boldsymbol{M}_1$ ($H_{\rm c1} \approx 8$ kOe for $K_1 = 1.2 \times 10^7$ erg/cm^3). Further increased negative magnetic field forces the magnetization of $\boldsymbol{M}_2$ even more parallel to $-z$ direction ($E \rightarrow F$), which results in a fully parallel magnetization configuration as shown in Fig.2(f). A similar switching process is observed in sweeping of magnetic field in the opposite direction (steps $F \rightarrow G \rightarrow H \rightarrow I \rightarrow A$), as shown in Figs.2(a) and 2(f)–2(i).

The observed magnetization rotation behaviour can be quantitatively analysed with a theoretical model. In the sandwich structure shown in Fig.1, the total energy per unit area E can be written as

$$\begin{aligned} E = {} & K_1 t_1 \sin^2\theta_1 + K_2 t_2 \cos^2\theta_2 - M_1 t_1 H \cos\theta_1 \\ & - M_2 t_2 H \cos\theta_2 + 2\pi M_1^2 t_1 \cos^2\theta_1 \\ & + 2\pi M_2^2 t_2 \cos^2\theta_2 - J_{\rm ex}\cos(\theta_1 - \theta_2), \end{aligned} \quad (2)$$

where K_i ($i = 1, 2$) is the uniaxial anisotropy of $\boldsymbol{M}_i$ (along z axis for i=1, along x axis for $i = 2$), M_i the saturation magnetization, θ_i the angle between $\boldsymbol{M}_i$ and the magnetic field $\boldsymbol{H}$, t_i the thickness. The term of $2\pi M_i^2 t_i \cos\theta_i$ is the effective demagnetization energy of $\boldsymbol{M}_i$. The last term is a weak exchange coupling between $\boldsymbol{M}_1$ and $\boldsymbol{M}_2$.

In order to give a quantitative interpretation for the magnetization response curve shown in Fig.2(a), we first define four characteristic fields: (i) positive saturation field (point B), where the magnetization of $\boldsymbol{M}_1$ and $\boldsymbol{M}_2$ are parallel above this field; (ii) zero applied field (point C), where the magnetization of $\boldsymbol{M}_1$ and $\boldsymbol{M}_2$ are perpendicular; (iii) coherent reversion field of $\boldsymbol{M}_1$ (points $D \rightarrow E$), where the switching from the antiparallel configuration to parallel configuration occurs; (iv) negative saturation field (point F).

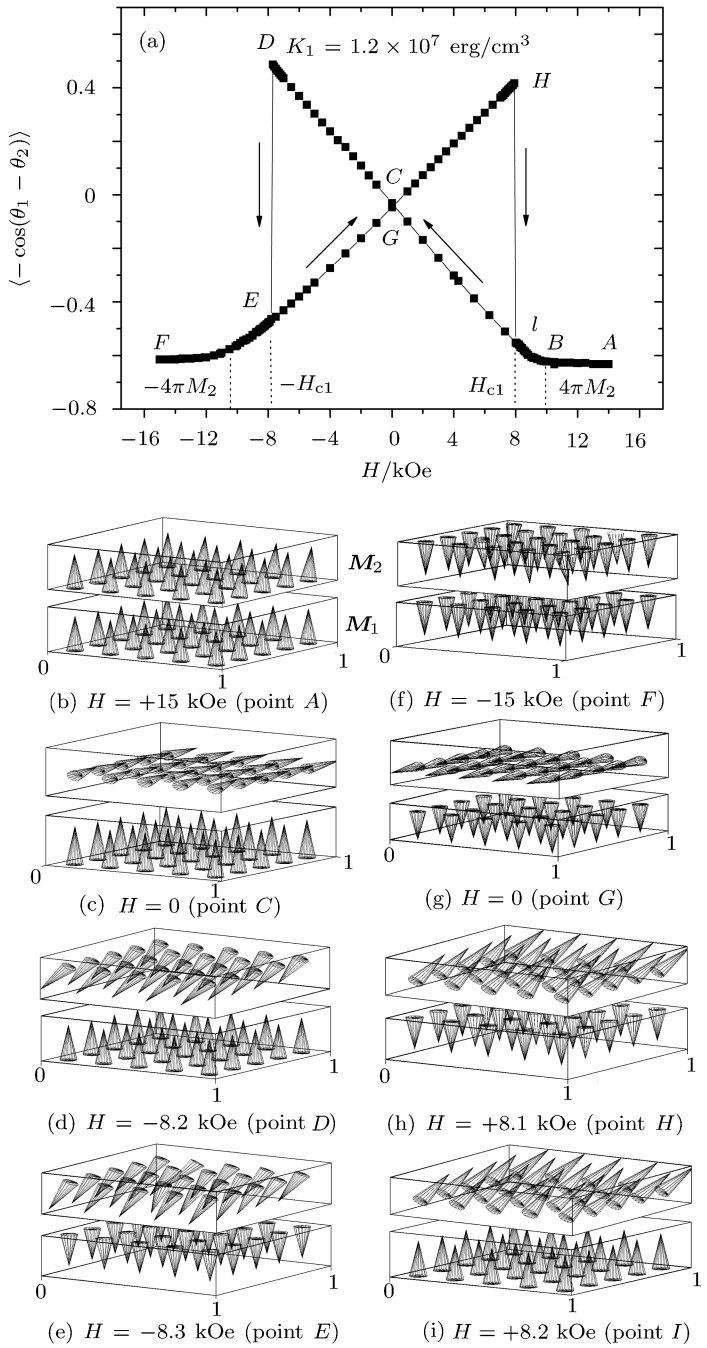


Fig.2. (a) Simulated GMR output in $\langle -\cos(\theta_1 - \theta_2)\rangle$ versus magnetic field for a high-field sensor. (b)–(i) Snapshots of magnetization configurations during the sweeping loop.

These characteristic fields can be analytically obtained by differentiating E of Eq.(2) with respect to θ_1 and θ_2 and then setting the derivative to zero at each characteristic point. The expressions of the partial derivatives of E read

$$\frac{\partial E}{\partial \theta_2} = M_2 t_2 H \sin\theta_2 - 2K_2 t_2 \sin\theta_2 \cos\theta_2 - 4\pi M_2^2 t_2 \sin\theta_2 \cos\theta_2 - J_{\rm ex}\sin(\theta_1 - \theta_2), \quad (3a)$$

$$\frac{\partial E}{\partial \theta_1} = M_1 t_1 H \sin\theta_1 + 2K_1 t_1 \sin\theta_1 \cos\theta_1 - 4\pi M_1^2 t_1 \sin\theta_1 \cos\theta_1 + J_{\rm ex}\sin(\theta_1 - \theta_2). \quad (3b)$$

By setting Eqs.(3a) and (3b) to zero, we obtain the following analytical expressions for the saturation field of $\boldsymbol{M}_2$:

$$H_{\rm sat} = (2K_2/M_2)\cos\theta_2 + 4\pi M_2 \cos\theta_2$$

$$+ (J_{ex}/M_2 t_2)\sin(\theta_1 - \theta_2)/\sin\theta_2, \quad (4a)$$

and for the coercive field of $\boldsymbol{M}_1$:

$$H_c = -(2K_1/M_1)\cos\theta_1 + 4\pi M_1\cos\theta_1 + (J_{ex}/M_1 t_1)\sin(\theta_1 - \theta_2)/\sin\theta_1. \quad (4b)$$

At characteristic field (i), since both θ_1 and θ_2 are approximately equal to 0 and the exchange field can be ignored because J_{ex} is typically of the order of 10^{-3} erg/cm^2, Eq.(4a) gives the critical saturation field $H^+_{sat} \approx 2K_2/M_2 + 4\pi M_2 \approx 10$ kOe. This value agrees with the simulated saturation field shown in Fig.2(a). Similarly, we can derive the negative saturation field (iv).

At zero field (ii), because the value of the perpendicular anisotropy field ($\sim$ 21 kOe) of $\boldsymbol{M}_1$ is about 1.6 times of demagnetizing field ($4\pi M_1 \sim 13$ kOe), a perpendicular magnetization configuration of $\boldsymbol{M}_1$ is retained. However, for the free layer $\boldsymbol{M}_2$, both the crystalline anisotropy and demagnetizing field drive it to an in-plane magnetization configuration. Therefore, we obtain the perpendicular magnetization configuration at zero field as shown in Figs.2(c) and 2(g).

Finally, we consider the switching field (iii) denoted by the points $D \to E$ in Fig.2(a), which has been recognized to be related to the reversal of $\boldsymbol{M}_1$ by the simulation. By putting $\theta_1 = 0$ and $\theta_2 \sim \pi$, the switching field (i.e. coercive field of $\boldsymbol{M}_1$) can be derived from Eq.(4b):

$$H_{c1} \approx -2K_1/M_1 + 4\pi M_1. \quad (5)$$

Eq.(5) yields $H_{c1} \sim -688$ kA/m for the parameters $K_1 = 1.2 \times 10^7$ erg/cm^3 and $M_1 = 1100$ emu/cm^3, which is quite close to the simulated value of -8 kOe.

We should point out that the field-sensing window is asymmetric (between $H^{\pm}_{sat}$ and $\mp H_{c1}$), as shown in Fig.2. The field-sensing window is defined as the linear region of the transfer curve. This is because $\boldsymbol{M}_1$ already reverses to $-z$ direction before $\boldsymbol{M}_2$ is fully saturated in $-z$ direction, see Figs.2(d). Thus, we can not obtain a completely antiparallel configuration. This result suggests that a symmetric field sensing window could be obtained by using material with even larger perpendicular anisotropy for $\boldsymbol{M}_1$ and/or by using material with lower moment for $\boldsymbol{M}_2$ (in order to decrease the demagnetization field $4\pi M_2$). Note that, the reduction of $4\pi M_2$ will inevitably decrease the sensing window, hence the enhancement of coercive field of $\boldsymbol{M}_1$should be a better solution to realize the symmetric window for large-field sensors.

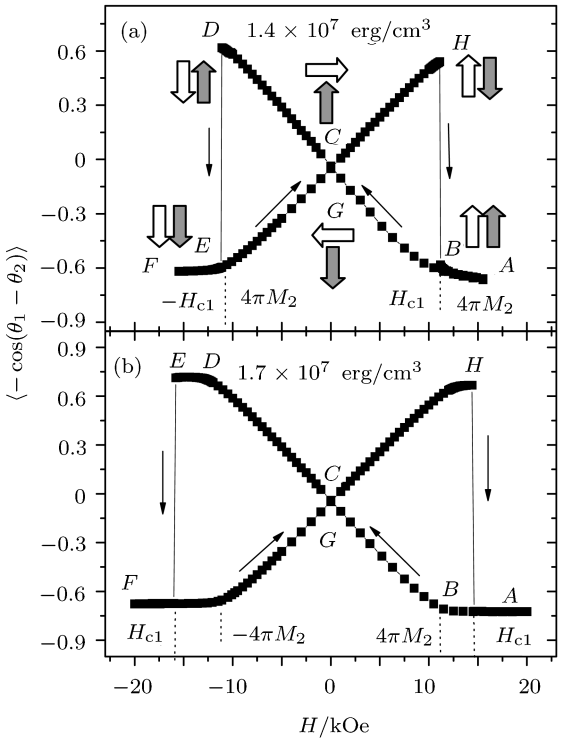


Fig.3. Simulated GMR output in $\langle -\cos(\theta_1 - \theta_2)\rangle$ for high-field sensors with a perpendicular anisotropy of $K_1 =$ 1.4 J/cm^3 in (a) and $K_1 = 1.7$ J/cm^3 in (b). Simulated magnetizations of $\boldsymbol{M}_1$ and $\boldsymbol{M}_2$ are sketched by dark and grey arrows, respectively.

Our simulations show that the coercive field of $L1_0$ FePt thin film is almost linearly dependent on the perpendicular anisotropy. Experimental results indicate that the perpendicular anisotropy can be obtained in range of $(1-7)\times 10^7$ erg/cm^3 by fine-tuning of deposition.[8] Simulation with larger perpendicular anisotropy for $\boldsymbol{M}_1$ was performed and the results are shown in Fig.3. Linear GMR outputs with symmetric sensing windows are observed for the field sweeping between +11 kOe and −11 kOe. The simulation is performed at zero temperature, without considering the thermal effect on the coercive field.[13] In Fig.3(a), the enhanced coercive field $H_{c1} \sim 11$ kOe at $K_1 = 1.4 \times 10^7$ erg/cm^3 is comparable to demagnetization field $4\pi M_s$ of $\boldsymbol{M}_2$, resulting in a completely antiparallel alignment at point D (or H). When the perpendicular anisotropy is further increased to $K_1 = 1.7 \times 10^7$ erg/cm^3, the simulated H_{c1} of $\boldsymbol{M}_1$ is increased to $\sim$ 15.8 kOe, which is larger than the demagnetization field of $\boldsymbol{M}_2$ ($\sim$ 11 kOe). Consequently, a flat plateau showing completely antiparallel configurations ($D \to E$) is observed in Fig.3(b).

4. Conclusion

In summary, spin-valve sensors capable of measuring high fields up to one Tesla have been investigated by micromagnetic simulation. The sensor studied consists of one ferromagnet with perpendicular anisotropy and another with in-plane anisotropy. The detailed magnetization configurations at different fields are presented. The simulation and quantitative interpretation indicate that the field sensing window is determined by the strength of the hard layer coercive field and the sense layer demagnetizing field.

References

[1] Tumanski S 2001 *Thin film Magnetoresistive Sensors* (London: Institute of Physics Publishing)

[2] Zhu T, Zhan W S, Shen F, Zhang Z, Xiang X H, Landry G and Xiao J Q 2003 *Chin. Phys.* **12** 665

[3] Li F F, Zhang X Q, Duan G X, Wang T X, Zeng Z M, Wei H X and Han X F 2005 *Acta Phys. Sin.* **54** 3838 (in Chinese)

[4] Zhang Z, Cardoso S, Wei P, Barradas N, Soares J C and Freitas P P 2001 *Appl. Phys. Lett.* **78** 2911

[5] Mamcoff F B, Dunn J H, Clemens B M and White R L 2000 *Appl. Phys. Lett.* **77** 1879

[6] Hehn M, Malinowski G, Sajieddine M, Jouguelet E and Schuhl A 2004 *Eur. Phys. J. Appl. Phys.* **28** 79

[7] Nishimura N, Hirai T, Koganei A, Ikeda T, Okano K, Sekiguchi Y and Osada Y 2002 *J. Appl. Phys.* **91** 5246

[8] Mangin S, Ravelosona D, Katine J A, Carey M J, Terris B D and Fullerton E E 2006 *Nat. Mater.* **5** 210

[9] Seki T, Mitani S, Yakushiji K and Takanashi K 2006 *Appl. Phys. Lett.* **88** 172504

[10] Liu Y W, Zhang Z Z, Zhang Z G., Freitas P P and Martins J L 2002 *J. Appl. Phys.* **91** 8296

[11] Liu Y W, Chen Y G, Yang Y P, Chen H and Martins J L 2005 *Chin. Phys. Lett.* **22** 1275

[12] Jin W, Liu Y W and Chen H 2006 *IEEE Trans. Magn.* **42** 2682

[13] Huang Z G, Chen Z G, Jiang L Q, Ye Q Y and Wu Q Y 2006 *Chin. Phys.* **15** 1602